Modeled Impact of Anthropogenic Warming on the Frequency of Intense Atlantic Hurricanes

Morris A. Bender, *et al.*

Science **327**, 454 (2010);
DOI: 10.1126/science.1180568

during the above desertification period had radiative forcing of +0.006 W m^{-2}, a factor of 24 smaller and in the opposite direction than the combined radiative effects [compare with (*28*)].

On the basis of our estimates, the total desertification in the semi-arid regions had a combined *RF* of about –0.14 W m^{-2}. This counteracts the equivalent of ~20% of the global *RF* associated with the 44-ppmv increase in atmospheric CO_2 over the same period [(*35*) e.g., (0.145–0.006)/0.62; see Eqs. 1 and 2], moderating the potential warming trend. This moderating effect adds to that assigned to the low CO_2 airborne fraction resulting from ocean and land carbon sinks (*34*). These are clearly first approximations, but the large effects and the large area involved with generally stable high-radiation low-cloud conditions make these estimates relatively robust and demonstrate again the importance of research in the semi-arid regions.

References and Notes

1. D. Baldocchi *et al.*, *Bull. Am. Meteorol. Soc.* **82**, 2415 (2001).
2. G. B. Bonan, *Science* **320**, 1444 (2008).
3. R. Lal, *Environ. Manage.* **33**, 528 (2004).
4. National Climatic Data Center, "Mean daily solar radiation, monthly and annual" (U.S. Department of Commerce, Washington, DC, 1964).
5. J. Otterman, *Science* **186**, 531 (1974).
6. J. Charney, W. J. Quirk, S. H. Chow, J. Kornfield, *J. Atmos. Sci.* **34**, 1366 (1977).
7. Y. K. Xue, *Q. J. R. Meteorol. Soc.* **123**, 1483 (1997).
8. Intergovernmental Panel on Climate Change (IPCC), *Fourth Assessment Report, Climate Change 2007: Synthesis Report,* available at www.ipcc.ch/publications_and_data/publications_ipcc_fourth_assessment_report_synthesis_report.htm.
9. M. Aubinet *et al.*, *Adv. Ecol. Res* **30**, 113 (1999).
10. K. Maseyk, J. M. Grunzweig, E. Rotenberg, D. Yakir, *Glob. Change Biol.* **14**, 1553 (2008).
11. K. S. Maseyk *et al.*, *New Phytol.* **178**, 603 (2008).
12. D. M. J. S. Bowman *et al.*, *Science* **324**, 481 (2009).
13. J. Penuelas, M. Boada, *Glob. Change Biol.* **9**, 131 (2003).
14. B. R. Helliker, S. L. Richter, *Nature* **454**, 511 (2008).
15. P. Ciais *et al.*, *Nature* **437**, 529 (2005).
16. G. Bala *et al.*, *Proc. Natl. Acad. Sci. U.S.A.* **104**, 6550 (2007).
17. R. A. Betts, *Nature* **408**, 187 (2000).
18. Four pairs of shortwave (0.29 to 4.0 μm, Kipp and Zonen CM21) and longwave (4.0 to 100 μm, Eppley precision infrared radiometer) radiation sensors were used, two (multiple positions) for measuring down- and upwelling radiation ~5 m above the canopy (and ~4 m away from the flux tower) and two (multiple positions) below the canopy ~1.5 m above bare soil surface. The L sensors output (precision mode) was corrected for solar radiation by using the companion S sensor. Albedo was estimated, in addition, from Moderate Resolution Imaging Spectroradiometer (MODIS) data for the forest and surrounding area using a full-year dark and white sky in the visible and near-infrared (NIR) spectral ranges (www-modis.bu.edu/brdf/userguide/albedo.html).
19. J. Charney, *Q. J. R. Meteorol. Soc.* **101**, 193 (1975).
20. G. L. Smith, A. C. Wilber, S. K. Gupta, P. W. Stackhouse Jr., *J. Clim.* **15**, 1175 (2002).
21. K. Fraedrich, A. Kleidon, F. Lunkeit, *J. Clim.* **12**, 3156 (1999).
22. M. Schaeffer *et al.*, *Global Biogeochem. Cycles* **20**, GB2020 (2006).
23. Aerodynamic resistance, r_a, was estimated as $r_a = \frac{H}{\Delta T_a} C_p \rho$. C_p and ρ are the air heat capacity and density; *H* was continuously measured; canopy-to-air temperature gradient, ΔT_a, was estimated from continuous sonic anemometer measurements 9 m above the canopy; and canopy "skin" temperature was estimated from upwelling longwave radiation measurements both above the soil and the canopy. For comparing forest and surrounding shrubland, surface temperatures were based on soil temperature measurements in the forest and at the shrubland (only 1 year for the latter), as well as MODIS surface temperature products for the forest and the surrounding region (at 10 km–by–10 km grids, 8-days mean at 10 AM, January through August 2005). Comparing roughness height was based on (*45*).
24. M. Claussen, V. Brovkin, A. Ganopolski, *Geophys. Res. Lett.* **28**, 1011 (2001).
25. G. Myhre, E. J. Highwood, K. P. Shine, F. Stordal, *Geophys. Res. Lett.* **25**, 2715 (1998).
26. A. Bar Massada, Y. Carmel, G. E. Tzur, J. M. Grünzweig, D. Yakir, *Can. J. For. Res.* **36**, 2585 (2006).
27. The time (*y*, years) required for a semi-arid forest to achieve balance between the surface positive *RF* and the carbon sequestration negative *RF* is approximated based on (*17*) as $y = \left(\frac{RF_{surface} \cdot \kappa \cdot C_0}{A_E \cdot NEE \cdot \eta \cdot \zeta}\right)$, where $RF_{surface}$ is either the albedo or the combined albedo-longwave effect, RF_{s+L}, A_E the Earth surface area (m^2), κ converts parts per million (ppm) CO_2 to kg C, C_0 the reference atmospheric CO_2 concentration (370 ppm), η is the CO_2 radiative forcing efficiency (W m^{-2}), ζ is the airborne fraction, and *NEE* is the observed annual net carbon uptake of the semi-arid forest (kg C m^{-2} $year^{-1}$).
28. E. L. Davin, N. de Noblet-Ducoudre, P. Friedlingstein, *Geophys. Res. Lett.* **34**, L13702 (2007).
29. H. N. Le Houérou, *J. Arid Environ.* **34**, 133 (1996).
30. S. Pacala, R. Socolow, *Science* **305**, 968 (2004).
31. G. P. Asner, J. M. O. Scurlock, J. A. Hicke, *Glob. Ecol. Biogeogr.* **12**, 191 (2003).
32. J. F. Reynolds *et al.*, *Science* **316**, 847 (2007).
33. Food and Agriculture Organization (FAO), *Carbon Sequestration in Dryland Soils* (World Soils Resources Reports 102, FAO, Rome, 2004).
34. J. G. Canadell *et al.*, *Proc. Natl. Acad. Sci. U.S.A.* **104**, 18866 (2007).
35. www.esrl.noaa.gov/gmd/ccgg
36. http://gaia.agraria.unitus.it/database/carboeuropeip/
37. W. J. Shuttleworth *et al.*, *Q. J. R. Meteorol. Soc.* **110**, 1163 (1984).
38. W. Knorr, K. G. Schnitzler, Y. Govaerts, *Geophys. Res. Lett.* **28**, 3489 (2001).
39. T. T. Warner, *Desert Meteorology* (Cambridge Univ. Press, Cambridge, 2004).
40. G. S. Campbell, J. M. Norman, *An Introduction to Environmental Biophysics* (Springer-Verlag, New York, ed. 2, 1998).
41. V. Masson, J. L. Champeaux, F. Chauvin, C. Meriguet, R. Lacaze, *J. Clim.* **16**, 1261 (2003).
42. J. Peixoto, A. Oort, *Physics of Climate* (Springer-Verlag, New York, 1992).
43. S. Luyssaert *et al.*, *Glob. Change Biol.* **13**, 2509 (2007).
44. T. Afik, thesis, Hebrew University of Jerusalem (2009).
45. R. H. Shaw, A. R. Pereira, *Agric. Meteorol.* **26**, 51 (1982).

46. We thank the students, postdocs, and technicians of the Yatir team for making this project possible. The long-term operation of the Yatir Forest Research Field Site is supported by the Cathy Wills and Robert Lewis Program in Environmental Science. Financial support from the Israel Science Foundation, Global Change and the Hydrological Cycle–Jordan River (GLOWA-JR), Keren Kayemet L'Israel (KKL), Jewish National Fund (JNF), the Minerva-Avron Center, and the Weizmann Institute is gratefully acknowledged.

31 July 2009; accepted 28 December 2009
10.1126/science.1179998

Modeled Impact of Anthropogenic Warming on the Frequency of Intense Atlantic Hurricanes

Morris A. Bender,[1]* Thomas R. Knutson,[1] Robert E. Tuleya,[2] Joseph J. Sirutis,[1] Gabriel A. Vecchi,[1] Stephen T. Garner,[1] Isaac M. Held[1]

Several recent models suggest that the frequency of Atlantic tropical cyclones could decrease as the climate warms. However, these models are unable to reproduce storms of category 3 or higher intensity. We explored the influence of future global warming on Atlantic hurricanes with a downscaling strategy by using an operational hurricane-prediction model that produces a realistic distribution of intense hurricane activity for present-day conditions. The model projects nearly a doubling of the frequency of category 4 and 5 storms by the end of the 21st century, despite a decrease in the overall frequency of tropical cyclones, when the downscaling is based on the ensemble mean of 18 global climate-change projections. The largest increase is projected to occur in the Western Atlantic, north of 20°N.

Rising sea-surface temperatures (SSTs) and a possible increase in Atlantic basin hurricane activity since 1950 have raised concern that human-caused climate change may be increasing Atlantic hurricane activity. Increasing amounts of greenhouse gases are a likely factor in the recent warming of tropical Atlantic SSTs (*1*–*3*), although internal variability (*4*) and reduced aerosol or dust forcing (*5*, *6*) may have also contributed. Some statistical analyses suggest a link between warmer Atlantic SSTs and increased hurricane activity (*6*–*8*), although other studies contend that the spatial structure of the SST change may be a more important control on tropical cyclone frequency and intensity (*9*–*11*). A few studies (*6*, *8*, *12*) suggest that greenhouse warming has already produced a substantial rise in Atlantic tropical cyclone activity, but others question that conclusion (*9*, *11*, *13*).

Dynamical models that can reproduce certain aspects of the observed frequency, structure, and intensity of hurricanes bring an important perspective to these questions (*9*, *10*, *14*–*16*). A recent modeling study (*16*) at the National Oceanic and

[1]National Oceanic and Atmospheric Administration/Geophysical Fluid Dynamics Laboratory, 201 Forrestal Road, Princeton, NJ, 08540, USA. [2]Center for Coastal Physical Oceanography, Old Dominion University, 4111 Monarch Way, Norfolk, VA 23508, USA.

*To whom correspondence should be addressed. E-mail: Morris.Bender@noaa.gov

Atmospheric Administration's (NOAA) Geophysical Fluid Dynamics Laboratory (GFDL) using an 18-km grid regional atmospheric model (ZETAC) has demonstrated success in reproducing the trend and year-to-year variability in August-through-October Atlantic tropical cyclone frequency during 1980 to 2005 [supporting online material (SOM) text]. The modeled interannual variability of hurricane counts was well-correlated with observed counts ($r = 0.86$) and exhibited an increasing trend during 1980 to 2005, although the modeled count was somewhat larger than what was observed.

Hurricane frequency in a globally warmed, late-21st-century climate was investigated in a subsequent study (*9*) by perturbing the mean atmospheric state and SSTs given in (*16*) by an ensemble-mean (18 models) late-21st-century climate change projection. The 18 models are from the World Climate Research Program coupled model intercomparison project 3 (CMIP3) (*17*) and use the Intergovernmental Panel on Climate Change (IPCC) A1B emissions scenario. The frequencies of both tropical storms and hurricanes in the ZETAC model were significantly reduced (–27% and –18%, respectively) in the warm climate relative to the control. However, the model was unable to simulate major hurricanes (category 3 to 5) with maximum winds greater than 50 m/s (Fig. 1B).

To improve the simulations of intensity, we extend the modeling approach of (*9*) by downscaling each individual model storm from that study with two different operational versions of the GFDL hurricane model (*18*). The National Weather Service (NWS) version of the model (termed here GFDL) has been used operationally since 1995, and since 2001, it has been coupled to a three-dimensional ocean model (*19*). The system has remained largely unchanged from 2006 through 2009 and has been run on a large sample of tropical cyclones of varying intensity. The second closely related version of this hurricane model (GFDN) has been run operationally by the U.S. Navy since 1996 for tropical cyclone activity globally. The GFDN model was upgraded in 2008 and uses modified surface physics compared with the GFDL version, providing a test of robustness of our results.

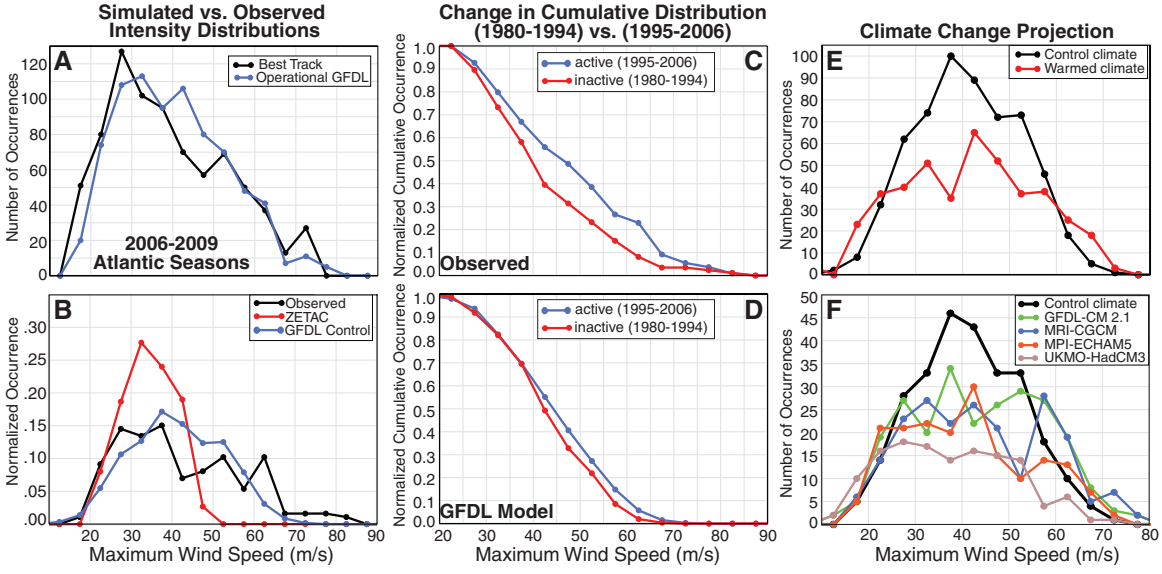

Fig. 1. Simulated and observed histograms of maximum surface wind speed (m/s) in the Atlantic basin. (**A**) Simulated versus observed maximum winds for every 120-hour forecast made (at 6-hour intervals) during the 2006 to 2009 hurricane seasons, using the GFDL operational model run by NOAA's NWS (excluding depressions). (**B**) Normalized intensity histogram (dividing by the total number of storms) for the ZETAC regional model (red), the combined GFDL (NWS) and GFDN (Navy) downscalings (blue), and the observed (black) for the 27 seasons (1980 to 2006) of the control simulations. (**C** and **D**) Observed (C) and simulated (D) cumulative maximum wind distribution (CDFs) comparing the period 1995 to 2006 (blue) to 1980 to 1994 (red). (**E**) Comparison of control (black) and warm climate (red) distributions (combined GFDL and GFDN models) based on the 18-member CMIP3 ensemble A1B scenario climate change. (**F**) Comparison of control (black) and warm climate (colors) distributions for the GFDL and GFDN models based on the four individual CMIP3 model A1B warming scenarios. To save computer resources, the four supplemental experiments (F) were only run for the 13 odd years during 1981 to 2005.

Table 1. Comparison of observed and control storm counts from the GFDL downscaling experiments for various categories of storm intensity and the percent change for each of the five warmed climate conditions. Results for all 27 years from 1980 through 2006 are shown in the leftmost three columns, with the columns indicated by asterisks computed for the 13 odd years only. The results are from the average of storm counts for the two versions of the operational hurricane model (versions run by NOAA's National Weather Service and the U.S. Navy). The warmed climate perturbation runs are based on downscaling the same seasons but with the addition of the mean climate change difference field between the 2001 to 2020 and the 2081 to 2100 periods from the CMIP3 model ensemble or the linear trend over 2000 to 2100 for each model, scaled to 80-year magnitude, for each of the four individual CMIP3 models (SOM text).

Type of storm	Number of observed storms (average storms per year)	Number of storms in control (average storms per year)	Ensemble warmed climate (every year; percent change)	Ensemble warmed climate* (percent change)	GFDL-CM2.1 warmed climate* (percent change)	MRI-CGCM warmed climate* (percent change)	MPI-ECHAM5 warmed climate* (percent change)	UKMO-HADCM3 warmed climate* (percent change)
Tropical storms and hurricane	9.0	10.9	–28%	–28%	–4%	–22%	–33%	–49%
Hurricane (33 m/s or above)	5.3	8.0	–32%	–33%	–7.5%	–24%	–40%	–60%
Major hurricane	2.4	2.7	–18%	–18%	40%	8%	–30%	–60%
Category 4 and 5	1.4	0.59	81%	75%	110%	110%	21%	–53%
Winds greater than 65 m/s	0.52	0.11	250%	220%	160%	180%	80%	–60%

Operational forecasts from the GFDL hurricane model have a distribution of maximum winds that agrees well with observations (Fig. 1A and fig. S1), and the model simulates a much more realistic distribution of intense hurricane winds than the ZETAC regional model does (Fig. 1B). To evaluate the GFDL model's ability to simulate the interdecadal variability of Atlantic hurricane intensities, we compared the observed and simulated cumulative distribution functions (CDFs) of maximum wind for the relatively inactive and active eras of 1980 to 1994 and 1995 to 2006 (Fig. 1, C and D). The observed CDF (Fig. 1C) is shifted toward higher intensities in the more-active era. The GFDL model (Fig. 1D) reproduces this tendency toward higher intensities, but underpredicts the magnitude of the change. The intensity distributions in Fig. 1, A and B, and the qualitative simulation in Fig. 1, C and D, of the multidecadal increase of hurricane intensity raises our confidence in the model's ability to simulate the effects of changes in the storm environment on intensity. However, the model's underprediction of the magnitude of the multidecadal intensity signal provides a note of caution. Future studies with significantly increased model horizontal resolution and explicit treatment of convection could potentially alter sensitivities to wind shear and other environmental conditions.

Despite the reduced storm frequency that was simulated in ZETAC (*9*), the distribution of maximum winds of the downscaled storms from the hurricane model shows an increase in the number of the most intense storms for the warmer climate compared with the control climate (Fig. 1E). Focusing on the category 4 and 5 hurricanes with maximum winds greater than 60 m/s, the total number (GFDN plus GFDL) increased sharply from 24 to 46. Hurricanes with winds greater than 65 m/s increased from 6 to 21.

Four individual CMIP3 global models were also downscaled using the same two-step methodology as is used in the 18-model ensemble. These four individual CMIP3 models (*17*) are the GFDL-CM2.1, the Japanese Meteorological Research Institute MRI-CGCM, the Max Planck Institute MPI-ECHAM5, and the Hadley Centre UK Meteorological Office UKMO-HadCM3. Because we used a single realization of the late-21st-century climate scenario (A1B) from each global model, the simulation results may differ between models in part because of internal variability, as well as because of differences in the global model formulations or precise forcings, although our experimental design attempts to reduce the influence of internal variability on the results (SOM text).

Figure 1F shows the intensity distributions obtained from downscaling the four individual CMIP3 models. The substantial differences between the resulting projections of intense hurricane activity imply that there are important differences among the large-scale environment changes projected by the 18-model ensemble (fig. S2) and by the individual models (fig. S3). The largest increase in category 4 and 5 hurricane numbers is simulated for the GFDL-CM2.1 and MRI-ECHAM5 models, with each exhibiting an increase of over 100% (Table 1), despite simulated reductions in the total number of hurricanes by 8% and 24%, respectively. On

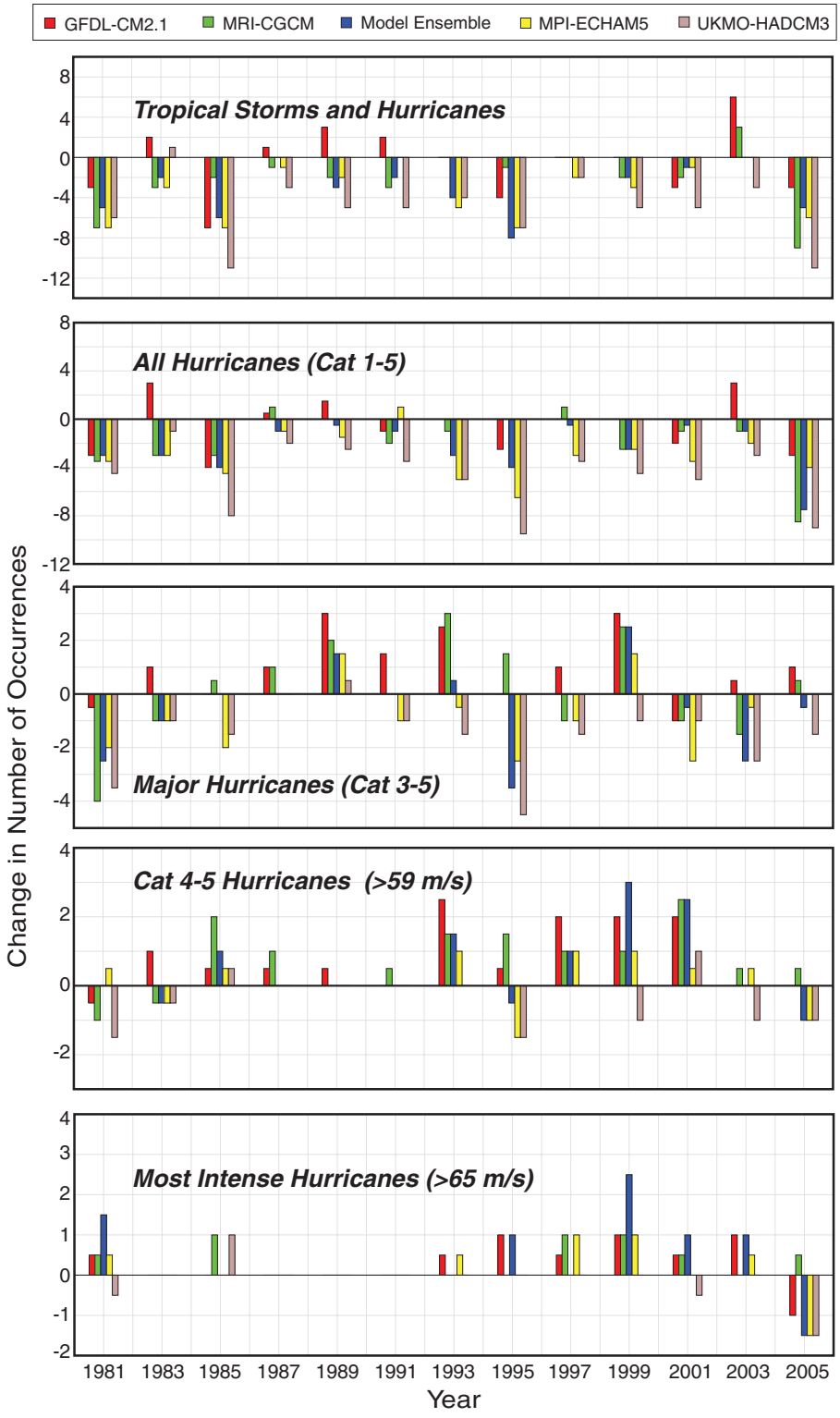

Fig. 2. Annual changes in storm counts for each odd year (1981 to 2005) warm minus control, for each of the five warmed climate scenarios. Results are shown for five categories of storm intensity (tropical storms and hurricanes, hurricanes, major hurricanes, category 4 and 5 hurricanes, and strong category 4+ hurricanes with maximum winds greater than 65 m/s). The five warmed climate scenarios plotted are the 18-model CMIP3 ensemble (blue), the GFDL-CM2.1 (red), the MRI-CGCM 2.3.2 (green), the MPI-ECHAM5 (yellow), and the UKMO-HadCM3 (gray). The results are computed from the average of storm counts for the two versions of the operational hurricane prediction model (GFDL and GFDN).

the other hand, the downscaling of the UKMO-HadCM3 produces a decrease in all categories of tropical cyclones. For the odd years, the most-intense simulated hurricanes (>65-m/s winds) in four of the five model projections (including the 18-model ensemble) showed an increase, ranging from 80 to 220%.

The year-by-year changes (warm minus control) of storm counts for each of the five downscaled climates were examined (Fig. 2). Results are presented separately for five different classes of storm intensity. Reduced numbers of both tropical storms and hurricanes are simulated nearly every year in the warm climate runs. For major hurricanes (category 3 to 5), a mix of increases and decreases is simulated, whereas for very intense hurricanes (category 4 and 5), a more robust increase in frequency results. Finally, the most intense hurricanes (>65 m/s) showed either no change or an increase in every year except one.

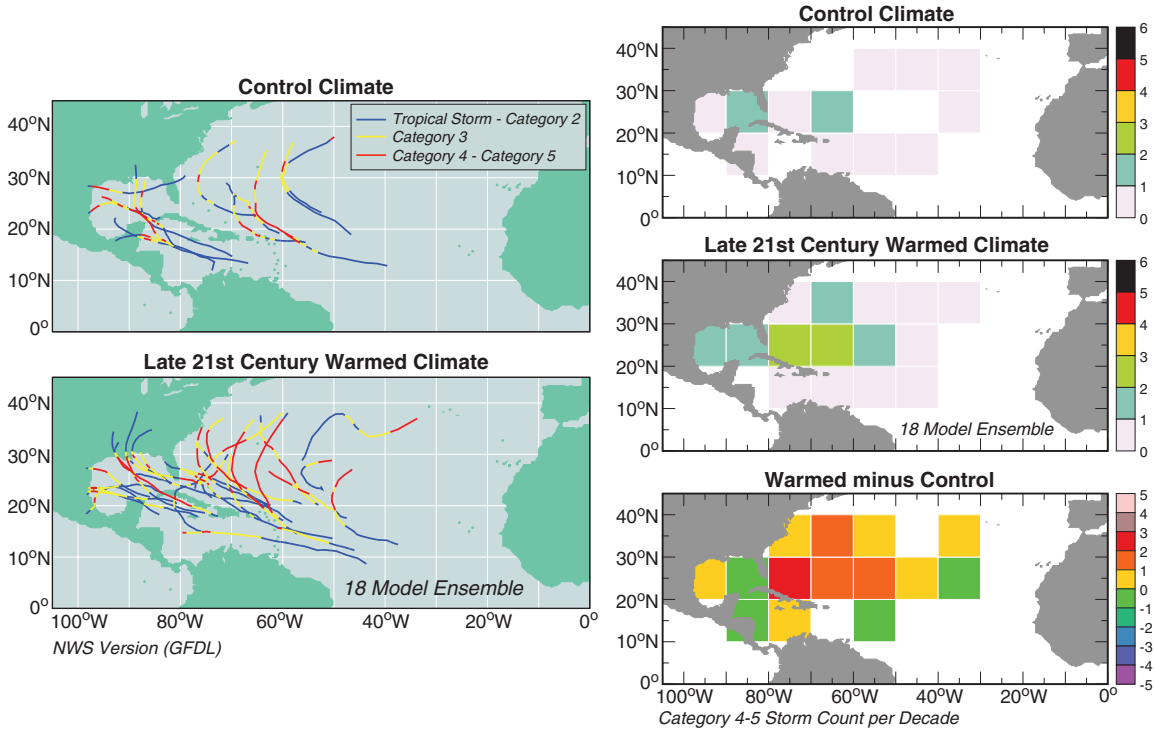

Fig. 3. (**Left**) Tracks for all storms reaching category 4 or 5 intensity, for the control and the warmed 18-model ensemble conditions, as obtained using the GFDL/NWS hurricane model. (**Right**) The spatial distribution of category 4 and 5 occurrences (scaled by storm counts per decade) for the combined control (average of the GFDL and GFDN model versions, top right); the combined CMIP3 18-model ensemble warmed climate results (middle right); and the difference between the warmed climate and control intense hurricane occurrences (bottom right). (The tracks for both the GFDL and GFDN models are presented in fig. S7 for comparison.)

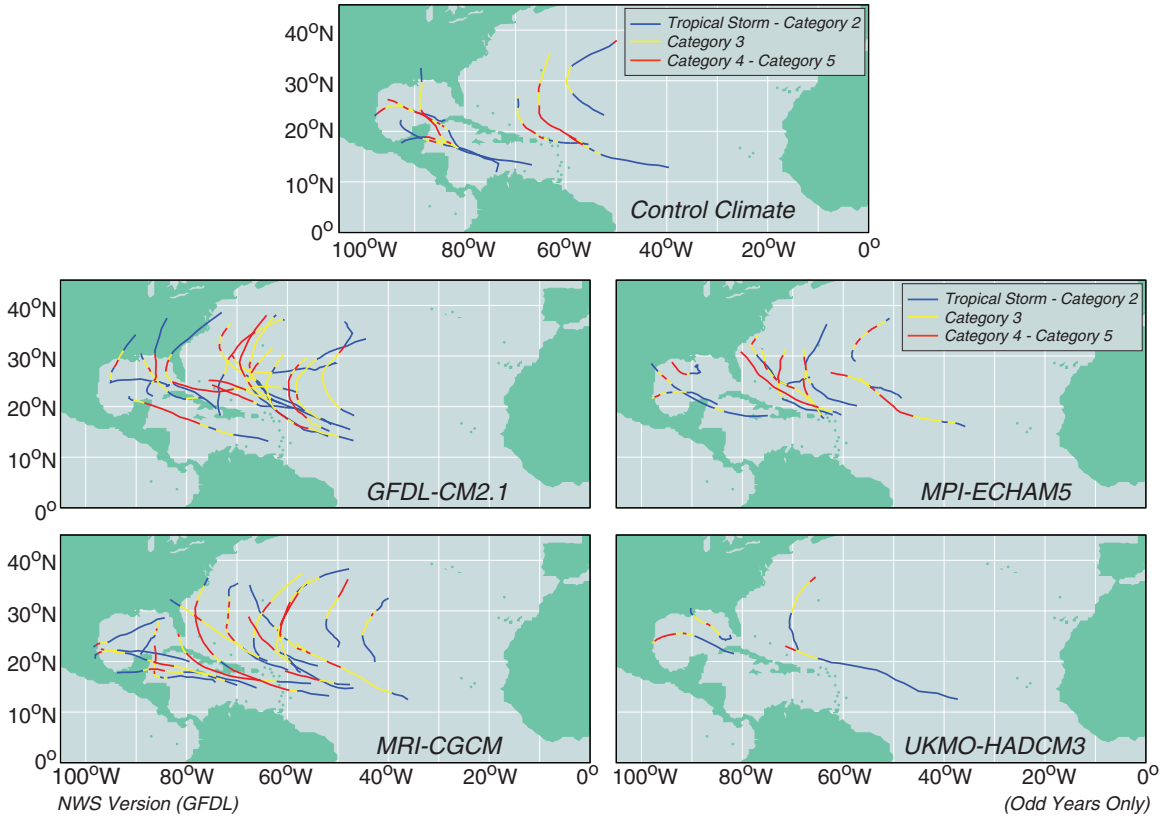

Fig. 4. Model tracks for all storms that eventually reached category 4 or 5 intensity, for the control (top) and the warm climate conditions provided by the four individual CMIP3 models. (The tracks shown are for the GFDL/NWS version of the hurricane model. For comparison, the results for the U.S. Navy's version of the model, GFDN, are presented in fig. S8).

The tracks and spatial distribution of category 4 and 5 hurricanes (Fig. 3) for the control and the warm climate (18-model ensemble) indicate that the largest increase of very intense hurricane activity is projected for the western Atlantic between 20°N and 40°N. This region corresponds fairly well with a region of increased potential intensity, reduced vertical wind shear, and increased SSTs (*20*) (fig. S2). In contrast, the ensemble mean exhibits an increase of shear in the Caribbean and mixed changes in the Gulf of Mexico (*20*) (fig. S2). The number of hurricane days for all categories, including category 4 and 5, decreases substantially in the Caribbean, with more modest decreases in the Gulf of Mexico (fig. S4).

The distribution of category 4 and 5 tracks and spatial distribution obtained from downscaling climate changes from the four individual CMIP3 models (Fig. 4 and fig. S6) show that for three of the four models, an increase of intense hurricane activity occurs in the region of the western Atlantic similar to the increase in the 18-model ensemble case. The decreased activity in the fourth model (UKMO-HadCM3) plausibly results from that model's relatively large projected increase in wind shear over much of the Atlantic south of 22°N (fig. S3), as well as a decrease in potential intensity in the western Atlantic equatorward of 25°N. In contrast, the GFDL-CM2.1 model projects reduced shear over most of the western Atlantic, whereas the MRI-CGCM and MPI-ECHAM5 models project shear changes (and simulated storm changes) between these two extremes. The differences between the individual GCM responses (fig. S3) and the ensemble-mean response (*20*) (fig. S2) give some indication of the uncertainty of the projected changes due to model formulation and/or forcing differences. Quantification of the relative influence of shear, potential intensity, or other environmental factors on these results is beyond the scope of this study.

The results in Figs. 3 and 4 used the GFDL/NWS version of the hurricane model. As a sensitivity test, the experiments were repeated using the alternative GFDN model. For both the 18-model CMIP3 ensemble (fig. S7) and the four individual CMIP3 models (fig. S8), the results are similar for the two operational models, increasing confidence in the robustness of our findings.

An analysis of normalized hurricane damage in the United States during 1900 to 2005 (*21*) indicates that major (category 3 to 5) and very intense (category 4 and 5) hurricanes at landfall accounted for 86% and 48% of all hurricane damage, respectively, despite accounting for only 24% and 6% of U.S. landfalls. Combining these findings with our model-based projections of the percent change in number of hurricanes for each category, we estimated changes in damage potential (table S1). For the CMIP3 ensemble mean and for two of four individual models, the increase in damage potential from the increase in very intense hurricanes outweighs the decrease in damage potential from the reduced occurrence of weaker systems. A damage potential increase of roughly 30% is projected for the CMIP3 18-model ensemble, with a range of roughly –50% to +70% among the four individual CMIP3 models. These estimates use projected storm changes over the entire North Atlantic basin. The estimate for the ensemble-mean CMIP3 model, in particular, would be increased if we took into account that the largest increase of intense hurricane frequency is projected for the western part of the basin.

For the downscaling of the 18-model CMIP3 ensemble-mean climate change, the frequency of category 4 and 5 hurricanes increased by 81% in 80 years (Table 1), corresponding to a linear trend of roughly +10% per decade. We estimate that the emergence time scale ($p = 0.05$) for such a linear trend would be roughly 60 years, based on bootstrap resampling tests using noise characteristics from the observed category 4 and 5 hurricane time series since 1944 (SOM text).

The A1B scenario for the 21st century includes significant reductions in aerosols as well as increases in greenhouse gases; we have not attempted to separate the effects of these two forcings in our projections. To the extent that aerosol effects are significant, rescaling these projections to historical periods with a different mix of aerosol and greenhouse gas forcings is problematic. We refer to the mix of forcings in the A1B scenario as "A1B-like."

Assuming that we can rescale our model projections to the observed (~0.5°C) tropical Atlantic warming since 1944, the expected increase in category 4 and 5 hurricanes from 1944 to 2008 due to A1B-like anthropogenic effects is only about +20%, or about one-third of the projected change at our estimated time of signal emergence. Although our internal variability estimate is very uncertain, these results suggest that one would not expect to detect an A1B-like anthropogenic influence on Atlantic basin category 4 and 5 frequency at the present time.

The observed category 4 and 5 time series for 1944 to 2008 (fig. S9), which incorporates a downward adjustment of intensities for certain storm classes during 1944 to 1969 (*22*), shows a pronounced increase since the 1970s. The frequency also increases by more than a factor of two, in terms of the estimated linear trend, over the period 1944 to 2008. We suspect, however, that the trend since 1944 is biased high because of changes in the capabilities of observing systems during the record, although a quantitative evaluation of such a bias is beyond the scope of this study. In addition to data problems (*13*, *22*), the potential influence on trends of Atlantic multidecadal variability (*4*) is cause for concern. If one has confidence in our downscaling results, and assumes that our A1B downscaling can be rescaled to apply to 1944 to 2008, this leads to a trend that is less than one-fifth of the observed magnitude. Such a small trend argues against the interpretation of the larger observed trend as resulting from a (rescaled) A1B-like anthropogenic forcing. On the other hand, our model's underestimate of the difference in intensity distributions between active and inactive periods (Fig. 1, C versus D) raises some note of caution concerning our model's estimate of anthropogenic intensity trends.

Our results suggest that a significant anthropogenic increase in the frequency of very intense Atlantic hurricanes may emerge from the background climate variability in the latter half of the 21st century, despite a projected decrease in the overall number of hurricanes. These findings are dependent on the global climate models used to provide the environmental conditions for our downscaling experiments. Future studies should reassess our findings using both updated climate model projections and improved hurricane simulation models.

References and Notes

1. S. Solomon *et al.*, Eds., *Climate Change 2007: The Physical Science Basis. Contribution of Working Group I to the Fourth Assessment Report of the Intergovernmental Panel on Climate Change* (Cambridge Univ. Press, Cambridge, 2007).
2. B. D. Santer *et al.*, *Proc. Natl. Acad. Sci. U.S.A.* **103**, 13905 (2006).
3. N. P. Gillett, P. A. Stott, B. D. Santer, *Geophys. Res. Lett.* **35**, L09707 (2008).
4. R. Zhang, T. L. Delworth, *Geophys. Res. Lett.* **33**, L17712 (2006).
5. A. T. Evan, D. J. Vimont, A. K. Heidinger, J. P. Kossin, R. Bennartz, *Science* **324**, 778 (2009).
6. M. Mann, K. Emanuel, *Eos* **87**, 233 (2006).
7. J. B. Elsner, J. P. Kossin, T. H. Jagger, *Nature* **455**, 92 (2008).
8. K. A. Emanuel, *Nature* **436**, 686 (2005).
9. T. R. Knutson, J. J. Sirutis, S. T. Garner, G. A. Vecchi, I. M. Held, *Nat. Geosci.* **1**, 359 (2008).
10. M. Zhao, I. M. Held, S. J. Lin, G. A. Vecchi, *J. Clim.*, **22**, 6653 (2009).
11. G. A. Vecchi, K. L. Swanson, B. J. Soden, *Science* **322**, 687 (2008).
12. G. J. Holland, P. J. Webster, *Philos. Trans. R. Soc.* **365**, 2695 (2007).
13. G. A. Vecchi, T. R. Knutson, *J. Clim.* **21**, 3580 (2008).
14. L. K. Bengtsson *et al.*, *Tellus* **59A**, 539 (2007).
15. S. Gualdi, E. Scoccimarro, A. Navarra, *J. Clim.* **21**, 5204 (2008).
16. T. R. Knutson, J. J. Sirutis, S. T. Garner, I. M. Held, R. E. Tuleya, *Bull. Am. Meteorol. Soc.* **88**, 1549 (2007).
17. G. A. Meehl *et al.*, *Bull. Am. Meteorol. Soc.* **88**, 1383 (2007).
18. M. A. Bender, I. Ginis, R. E. Tuleya, B. Thomas, T. Marchok, *Mon. Weather Rev.* **135**, 3965 (2007).
19. M. A. Bender, I. Ginis, *Mon. Weather Rev.* **128**, 917 (2000).
20. G. A. Vecchi, B. J. Soden, *Geophys. Res. Lett.* **34**, L08702 (2007).
21. R. A. Pielke *et al.*, *Nat. Hazards Rev.* **9**, 29 (2008).
22. K. Emanuel, *J. Clim.* **20**, 5497 (2007).

23. We wish to thank T. Marchok, R. Stouffer, A. Wittenburg, and three *Science* reviewers for their helpful comments and suggestions on earlier versions of the manuscript. We are also grateful to T. Marchok for his assistance in the preparation of several figures and to S. Sellars for assistance with some statistical calculations. Special appreciation goes to the current director of GFDL, V. Ramaswamy, for his support and encouragement. We thank the CMIP3 modeling groups, the Program for Climate Model Diagnosis and Intercomparison (PCMDI), and the World Climate Research Programme's (WCRP) Working Group on Coupled Modelling (WGCM) for their roles in making available the WCRP CMIP3 multi-model dataset. Support of this dataset is provided by the Office of Science, U.S. Department of Energy.

Supporting Online Material

www.sciencemag.org/cgi/content/full/327/5964/454/DC1
Materials and Methods
SOM Text
Figs. S1 to S9
Table S1
References

13 August 2009; accepted 23 November 2009
10.1126/science.1180568